Pergamon

0301-9322(95)00045-3

Int. J. Multiphase Flow Vol. 21, No. 6, pp. 1047–1062, 1995

0301-9322/95 $9.50 + 0.00

MEASUREMENT OF BUBBLE SIZE, VELOCITY AND CONCENTRATION IN FLASHING FLOW BEHIND A SUDDEN CONSTRICTION

J. DOMNICK and F. DURST

Lehrstuhl für Strömungsmechanik, Universität Erlangen-Nürnberg, Cauerstr. 4, 91058 Erlangen, Germany

(Received 7 October 1993; in revised form 17 May 1995)

Abstract—In the present paper the results of investigations in flashing flow behind a sudden constriction in vertical upflow are described. Flow visualization, laser-Doppler and phase-Doppler anemometry have been used to measure local bubble and fluid velocities, local bubble sizes and void fractions. The measurements were performed in the midplane of a two-dimensional channel with a 2:1 stepwise constriction.

It was found that bubble nucleation takes place in the recirculation zone immediately behind the constriction, which is the location of the lowest static pressure. These bubbles are transported downstream by the mean flow field, while undergoing further growth. No additional nucleation was observed downstream of the recirculation zone. A periodic, cloudwise behaviour of the bubble formation was found which could be explained by the interaction between the bubble growth and the mean flow field. This interaction results in strong disturbances of the mean flow field, which show up as an increase of the fluctuating bubble velocity by a factor of 3 compared to single-phase measurements in a region of 10 step heights behind the constriction. However, these fluctuations appear more like a periodic change in the mean velocity rather than a higher turbulence level. The measured arithmetic mean bubble diameters rise from approx. 50 μm in the recirculation region to about 70–80 μm 50 step heights downstream. Maximum local bubble number density and void fraction were found to be 16000 l/cm^3 and 0.8%, respectively.

Key Words: flashing flows, phase distribution, channel flow, sudden constriction

1. INTRODUCTION

The prediction of bubble size, bubble number density and void fraction in flashing flows is a very important factor in nuclear safety considerations, e.g. in case of LOCA (loss-of-coolant-accident), where flashing flow occurs due to rapid depressurization of the liquid. Critical flow is reached in the smallest passage of the leakage or downstream of it. The critical mass flux, which depends on the void fraction at the location of the blockage, defines the remaining emergency cooling time. The development of the void fraction in the streamwise direction depends on the location and the density of the initial bubble nucleation and further bubble growth, which is, in turn, influenced by the pressure gradient along the flow. Riznic *et al.* (1988) have formulated a one-dimensional equation which describes the development of the bubble number density N_b as a function of the axial coordinate z in the following way:

$$\frac{\partial N_b}{\partial t} + (\nabla \cdot N_b \mathbf{u}) = \Phi_{so} + \Phi_{si} \qquad [1]$$

$(\nabla \cdot N_b \mathbf{u})$ is the divergence of the vector $N_b \mathbf{u}$ and $\mathbf{u}$ the local bubble velocity. Φ_{so} and Φ_{si} are bubble source and sink terms due to nucleation and collapse or coalescence, respectively. This equation can be further simplified assuming steady state flow conditions. After integration from z_s, which is the axial coordinate where the onset of nucleation takes place, to a coordinate z_1, the final equation

$$N_b(z_1) = \frac{1}{A(z_1)u_z(z_1)} \int_{z_s}^{z_1} \Phi_w A(z)\, dz \qquad [2]$$

describes the local bubble number density at z_1. A is the cross-sectional area, u_z the velocity in axial

direction and Φ_w the bubble nucleation rate on the wall. In this equation, it is assumed that the major bubble growth is due to heterogeneous nucleation at the wall. As a first step towards the solution of this equation, the following parameters must be determined:

(1) flow conditions at the onset of nucleation
(2) nucleation site densities at the wall
(3) bubble departure frequency.

However, since [2] also contains the local axial mean velocity $u_z(z_1)$, which, in turn, depends on the actual void fraction, this equation can only be solved iteratively. To determine the void fraction as a function of the axial coordinate, additional parameters like

(4) bubble departure size
(5) bubble growth as a function of z-coordinate
(6) local bubble size distribution
(7) velocity of sound in the case of non-equilibrium

must be introduced into the computations and are either estimated from theoretical considerations or taken from measurements. Nevertheless, results of the axial development of the integral void fraction experimentally obtained by Reocreux (1974) and Abuaf *et al.* (1981) in convergent–divergent nozzles have been reproduced with some success.

Recently Bilicki *et al.* (1990) have published a new interpretation of the results from Reocreux. In addition to the one-dimensional equations for mass, momentum and energy conservation they formulated another equation for the quality. Introducing a process relaxation time the presence of local thermodynamic non-equilibrium is taken into account. From this equation, the void fraction can be derived considering the assumptions of the homogeneous model.

From these two exemplary theoretical descriptions of flashing flow it becomes evident that there is a need for local measurements. These measurements should deliver bubble size distributions, bubble velocities and bubble number densities with a high spatial resolution. With this information a large improvement in the description of the first stage of flashing flow, i.e. the bubble departure size, departure frequency and the evolution of bubble number density, would be possible. Furthermore, it has been shown previously, that the correct simulation of these initial processes is a keypoint for the success of the simulation of the whole flow. It was the intention of the present investigation to look into the initial bubble dynamics in flashing flow and to obtain the interaction between the developing second phase and the homogenous flow field.

Several publications concerning investigations of vertical two-phase channel flows are available, e.g. Sadatomi *et al.* (1982). However, most of these publications deal with water–air flow at void fractions, which are at least one order of magnitude larger. Therefore, some of the obtained characteristics, e.g. bubble interaction or coalescence, are not relevant in the present investigation. Moreover, it cannot be expected to reach a fully developed two-phase channel flow herein.

2. EXPERIMENTAL TEST FACILITY

2.1. Two-phase flow loop

To investigate a two-phase flashing flow, a closed flow loop was constructed which contained Freon 12 as test fluid. Freon 12 was chosen due to its low critical pressure and temperature ($p_{cr} = 41.5$ bar, $T_{cr} = 112^{\circ}$C), allowing experiments with evaporation under moderate pressure and temperature conditions. Furthermore, for this fluid all necessary properties, including the temperature dependency of the refractive index, are known to an accuracy sufficient for the present investigations. Figure 1 shows schematically the major parts of the flow loop with the test section (5) being the central part. The flow through the test loop was provided by means of a hermetically sealed centrifugal pump (1), mounted at the lowest point of the loop. The water-cooled condenser (6), located at the top of the loop, was directly connected to the pump at the bottom to ensure single-phase flow in the feed line to the pump. Since this pump always ran at full speed, a bypass line was installed parallel to the main line and the flow rate was controlled by two regulating valves

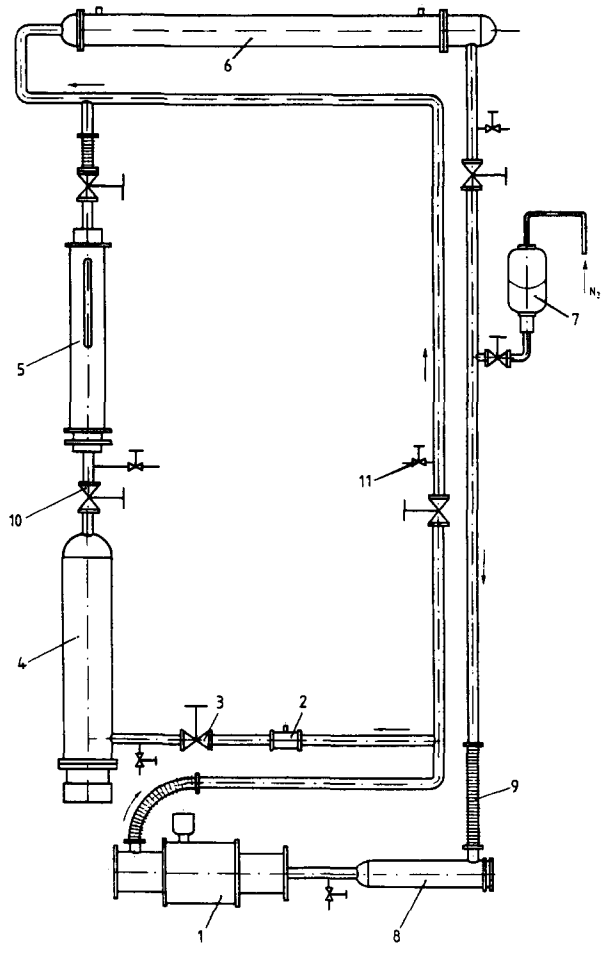

Figure 1. Two-phase flow test rig.

(3). Each element of the loop could be separated from the rest by means of isolation valves (10) to allow an easy exchange of individual parts without draining the whole test loop.

Design pressure and temperature were chosen according to the critical point of Freon 12. The maximum volume flow rate of the vertically mounted loop was 360 l/min. The flow rates could be kept constant within $\pm 0.5\%$. The whole flow loop was fabricated from stainless steel, since preliminary single-phase measurements of the flow in the test section were performed with water. By means of an 80 kW electrical preheater (4) the liquid could be heated up to a preset temperature at the entrance to the test section. A pneumatic pressurizer (7) to the flow loop allowed independent control of pressure and temperature, so that the thermodynamic state of the liquid could be adjusted easily. At several locations the loop was instrumented with pressure transducers and thermocouples and the readings of these sensors were fed into a microcomputer which performed an on-line control of the thermal and hydraulic state of the loop.

2.2. Test section

Since the presented experiments form the basis of numerical flow simulations using a two-dimensional Euler/Lagrange particle tracking approach, a two-dimensional geometry had to be chosen as test section. This test section had to withstand a 40 bar design pressure as well as permitting optical access to the whole flow field. A flat channel with a 2:1 constriction and an aspect ratio of 15:1 was constructed from stainless steel with borosilicate glass windows of 30 mm thickness arranged on both smaller sides over a length of approximately 300 mm on both sides of the constriction. As will be explained later, a third window was located on one side in the midplane of the larger side of the channel to give optical access to the flow under 90°. Figure 2 shows a

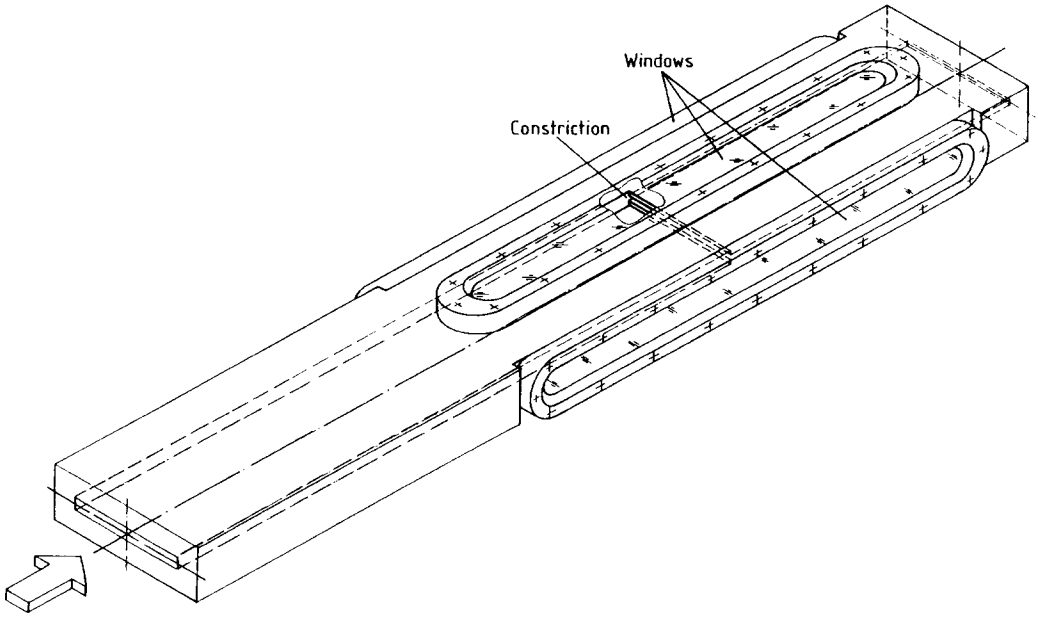

Figure 2. Test section.

perspective view of the channel, indicating that the channel constriction was roughly located in the middle of the windows.

The cross section of the channel upstream of the constriction was 15 × 1 cm. The height was reduced to 5 mm behind the constriction. The dimensions of the channel were chosen as a compromise between the total size of the flow loop, which scales with the test section size, and the spatial resolution of the optical measuring techniques used. The inner surface of the channel was ground and polished with a remaining surface roughness of approximately 10 μm. During assembly special care was taken to keep the surface clean and undamaged. The channel was equipped with 5 pressure taps, each 0.5 mm in diameter, to monitor the pressure distribution along the channel. The first pressure tap located 100 mm upstream of the constriction provided a reference pressure and was equipped with a high precision pressure transducer with an accuracy of $\pm 0.01\%$ of the actual reading. In this way the thermodynamic state of the fluid was well known when it entered the region of investigation.

3. APPLIED MEASURING TECHNIQUES

The parameters that were supposed to be measured in the initial range of flashing flow can be summarized as follows:

(1) mean and rms velocity of the homogeneous phase
(2) mean and rms velocity of the growing bubbles
(3) local bubble size distribution, bubble number density, void fraction and interfacial area concentration
(4) correlation between bubble size and velocity.

Phase-Doppler anemometry can provide this information for spherical particles with a high accuracy (e.g. Durst *et al.* 1975; Bauckhage *et al.* 1984; Bachalo *et al.* 1984). Furthermore, it was already successfully applied to cavitating flows by Saffman *et al.* (1984) and Tanger *et al.* (1989). However, as will be shown in the next chapter, fundamental investigations of the scattered light field were necessary to adapt the phase-Doppler technique to bubbly flows of Freon 12, taking into account the existing knowledge of the refractive index of the fluid.

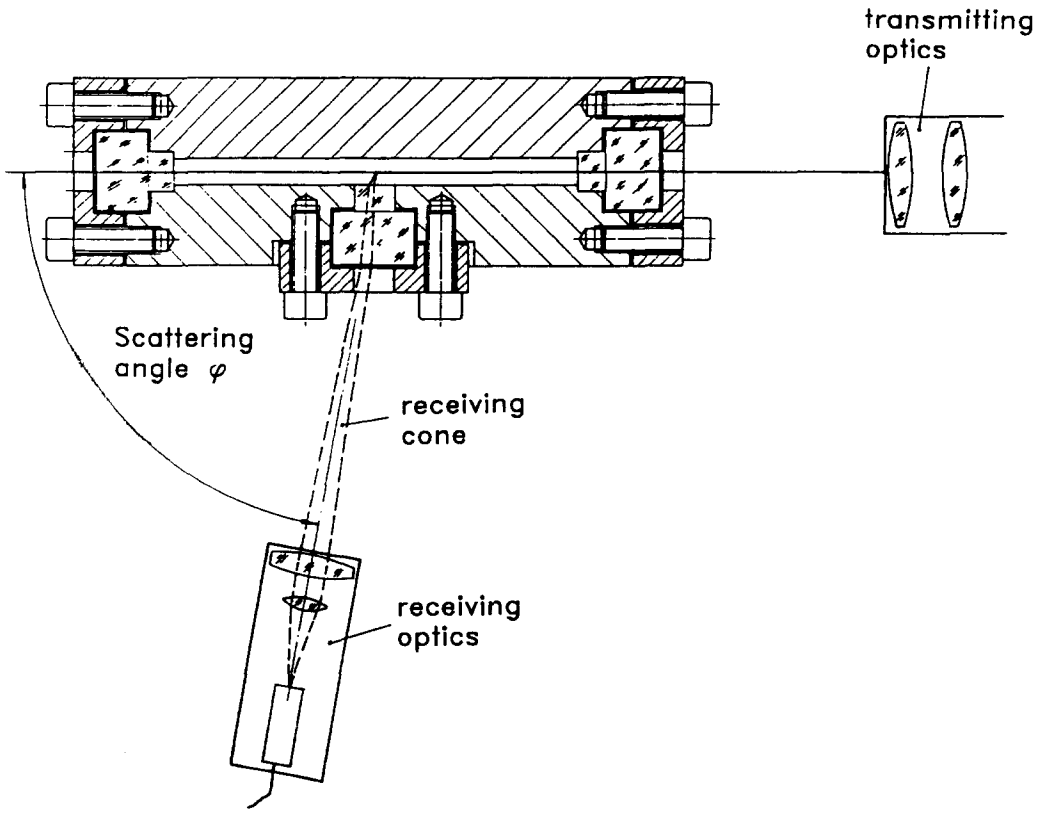

Figure 3. Geometrical arrangement of the phase-Doppler system.

3.1. *Laser-Doppler and phase-Doppler anemometry*

A standard single-component forward scatter LDA was used in the initial measurements yielding velocity information of the single-phase flow. The optical system consisted of a 10 mW HeNe Laser, a beamsplitter providing a 25 mm laser beam separation, a double Bragg cell module to yield the appropriate optical shift and a 300 mm transmitting lens focusing the laser beams in the probe volume. The resulting probe volume size was 200 μm in diameter and 3 mm in length. A 300 mm receiving lens was used to focus the scattered light on to a photomultiplier tube. A DANTEC counter was employed for signal processing. For all measurements in single-phase flow a shift frequency of 500 kHz was chosen, corresponding to a velocity offset of 5.1 m/s.

A different transmitting system was set up for the PDA measurements. While using the same 10 mW HeNe laser, the beam splitting and Bragg cell sections were replaced by a rotating diffraction grating system, delivering two expanded 3 mm beams with a spacing of 14.8 mm at the 310 mm focal length front lens. Therefore, the final probe volume diameter was only 80 μm. The probe volume length, which in a sideward scatter arrangement is defined by the size of the receiving slit image in the probe volume, was 800 μm. A shift frequency of 0.41 MHz was used throughout all the PDA measurements. The receiving optics was a simple two detector system with a 310 mm receiving lens (diameter 80 mm) and two 80 mm focusing lenses (diameter 30 mm) at 40 mm spacing. Figure 3 shows a cross-sectional view of the PDA system arranged around the test section.

Since phase-Doppler measurements of the particle size are only possible if one scattering mechanism is dominant, an appropriate scattering angle must be selected taking into account the effective geometry of the transmitter, the properties of the receiving optics and the complex refractive index of the particle phase, i.e. bubbles. This selection was done by means of a Mie-scattering program (Naqwi & Durst 1989). The real part of the refractive index was taken from Pfeiffenberger *et al.* (1978), who reported values for Freon 12 bubbles in liquid Freon of 0.78 at 20°C and 0.80 at 40°C. The absorption coefficient was measured in the present study and was found

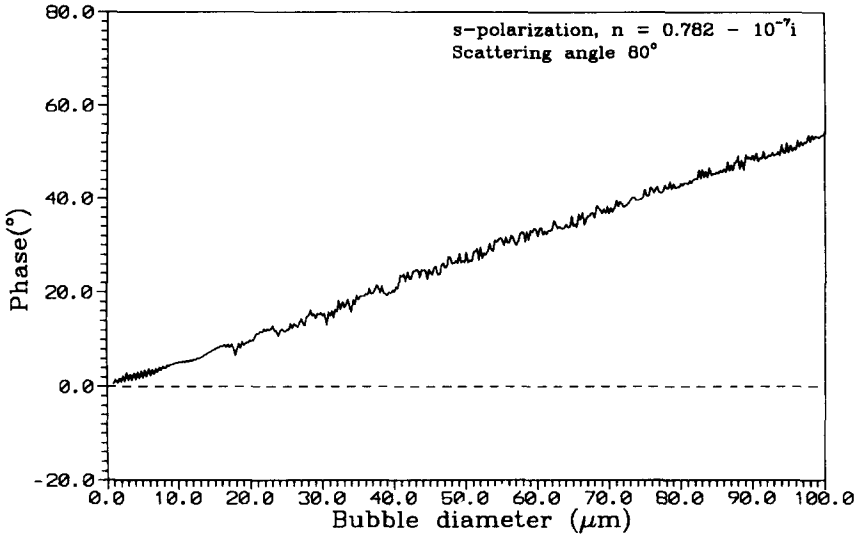

Figure 4. Phase-Doppler response curve for Freon 12.

to be practically 0. Due to geometrical limitations of the test section, only scattering angles between 75 and 105° were possible. The final result of the Mie calculations is shown in figure 4. In this figure, a good linearity of the phase–size relationship can be seen for light polarized parallel to the plane of the transmitting beams at a scattering angle of 80°. Phase oscillations, which are present in the whole size range, do not exceed 4°. However, these oscillations increase rapidly with increasing

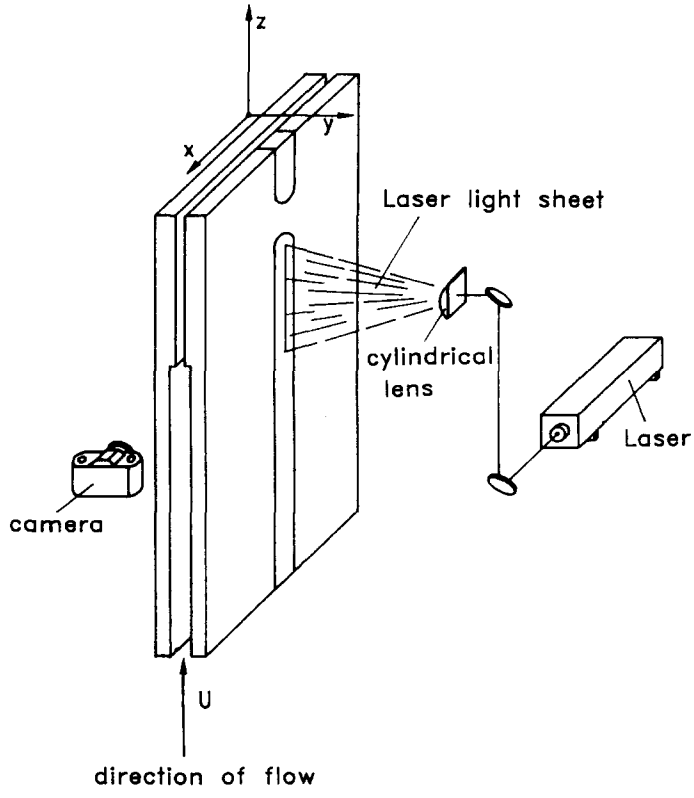

Figure 5. Arrangement of the laser light sheet technique.

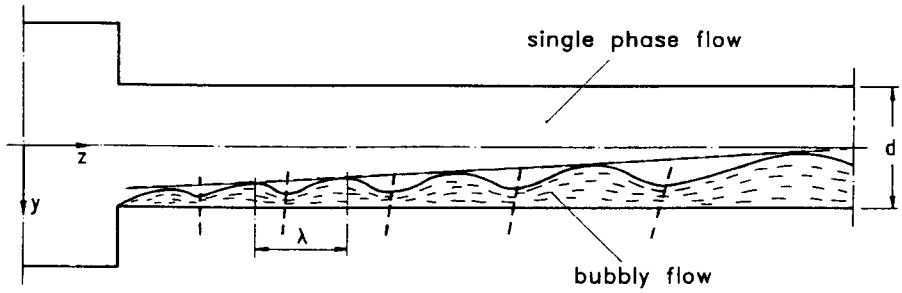

Figure 6. Axial development of the bubble zone.

temperature, since the relative refractive index approaches unity. Calculations have shown that with the final arrangement PDA measurements in Freon 12 are limited to temperatures up to 50°C.

In the final measurements, it was found that reflections from the back surface of the channel led to a decrease in SNR. Therefore, the receiving optics was raised above the normal scattering plane by an angle of approximately 5°. Nevertheless, the very robust and accurate cross-spectral density method (Domnick *et al.* 1988), best suited for signals with low SNR, had to be used to obtain reproducible results.

3.2. Flow visualization

Supplementary to the local LDA and PDA measurements, flow visualization studies were made to obtain the overall flow field structure in the region near the constriction. A laser light sheet with a thickness of approximately 0.5 mm was placed in the midplane of the channel through the side window, while photographic pictures or video tapes were recorded under a 90° observation angle. For some measurements, a triggered Bragg cell was used to deflect the laser beam into a beam stop to achieve exposure times around 1 μs for highly time-resolved photographic records of the flow. Figure 5 shows the arrangement of the laser light sheet measurements, indicating in which direction the photographic studies were carried out.

For some initial measurements the flow visualization technique was extended to particle sizing to obtain comparative bubble size measurements method. Transforming the locally resolved temporal mean values obtained by the phase-Doppler into spatially averaged values a very good agreement was found between the two methods with differences less than 5% in the arithmetic mean diameter.

4. EXPERIMENTAL RESULTS

Measurements in various flashing flows were made at temperatures between 15 and 35°C, corresponding to saturation pressures of Freon 12 between 4.9 and 8.5 bar. The examined mass fluxes ranged between 3500 and 6000 kg/m^2/s with Re numbers, based on the bulk velocity and the channel height, between 50,000 and 130,000. The general flow structure, obtained with the laser light sheet technique, is shown in figure 6. The observations can be summarized as follows:

- Bubble nucleation and growth take place in the small recirculation zone immediately after the constriction. The length of this zone is approximately 4.5 mm.
- In spite of the static pressure increasing after the vena contracta, bubbles do not collapse. As was confirmed by the PDA measurements to be presented later, the bubble number density remains almost constant downstream of the constriction.
- A periodic appearance of bubble clouds can be seen providing characteristic wavelengths.
- Downstream of the constriction, the bubble zone expands due to the turbulent motion in the channel. Approximately 6 channel heights from the constriction the first bubbles reach the channel centerline.
- At the investigated mass fluxes between 3500 and 6000 kg/m^2/s, the first bubbles occur at static pressures of 200 mbar higher than the saturation pressure, measured at a distance of

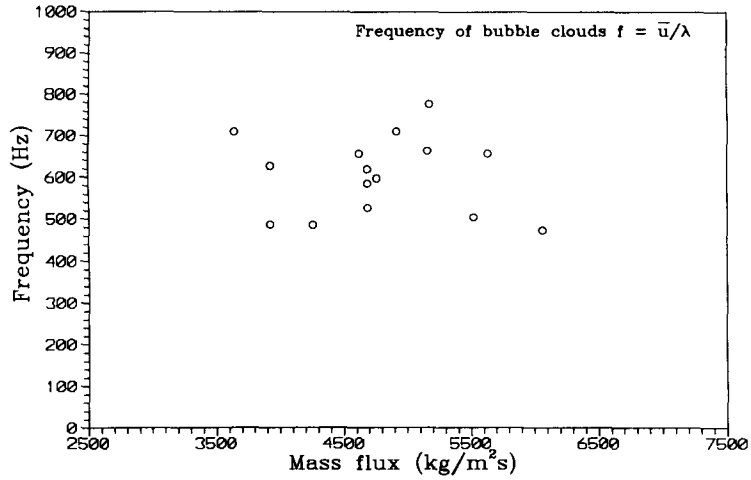

Figure 7. Observed "bubble cloud" frequencies.

100 mm upstream of the constriction. It can be assumed that at this condition saturation pressure is reached in the recirculation zone.

- Flashing occurs preferentially on the stainless steel channel wall, By further decreasing the static pressure in the channel a more symmetric bubble zone could be obtained.

The frequency of the "bubble clouds" was calculated from the measured wavelength and the bulk velocity. As shown in figure 7, these frequencies are almost independent of the mass flux or the bulk velocity. Therefore, it can be concluded that this periodic behaviour is the result of the bubble growth process, which has a time constant depending only on the evaporation process at the location of bubble creation rather than on the flow field. The increasing volume in the recirculation zone, due to the bubble growth, leads to an increase of the size of this recirculation zone and subsequent "hydraulic non-equilibrium". After reaching a certain threshold size, the whole recirculation zone is transported away by the mean flow and the process starts again. As will be shown later, this periodic process creates an additional fluctuating velocity component in the channel flow, which is measurable even 40 channel heights downstream of the constriction. The

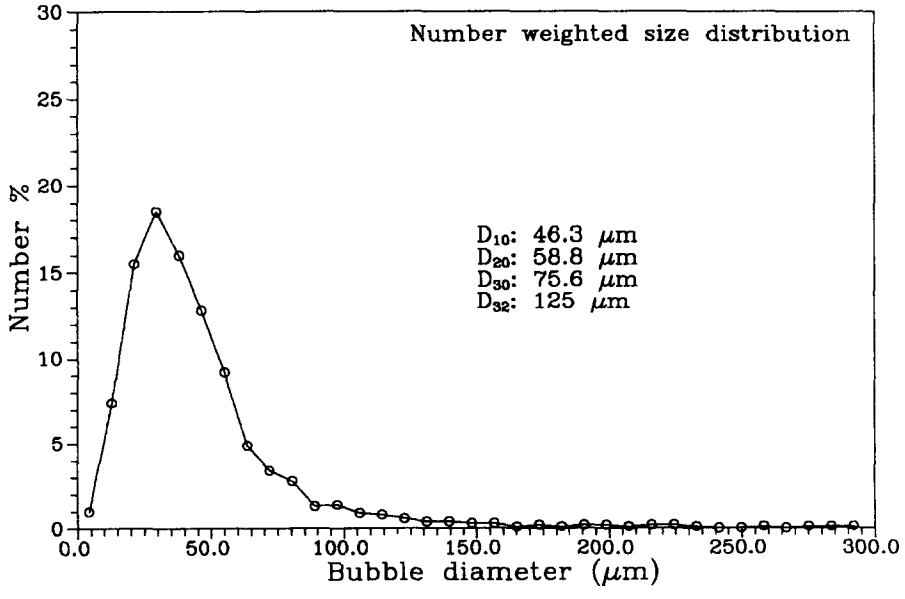

Figure 8. Measured local number weighted size distribution.

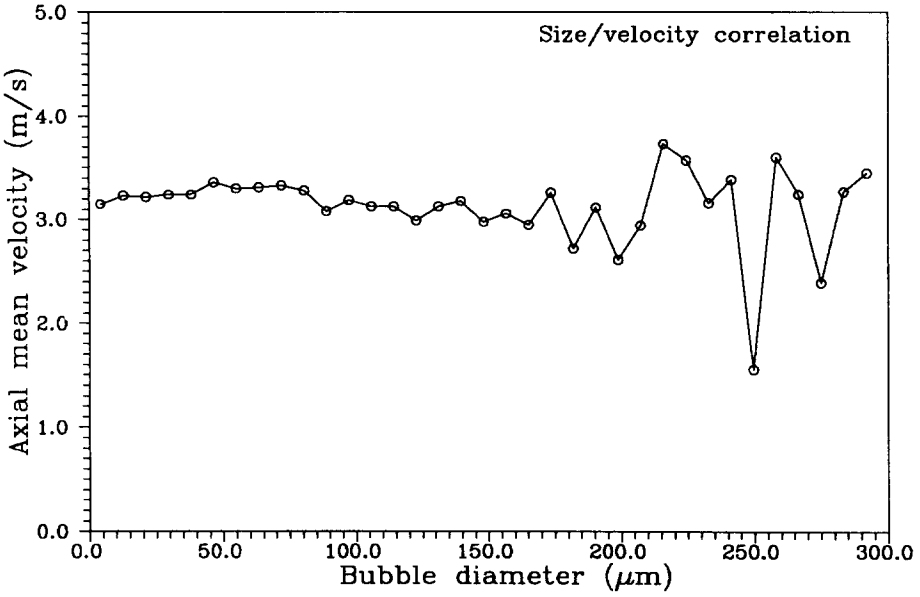

Figure 9. Measured local size–velocity correlation.

observed frequencies between 500 and 800 Hz indicate, that bubble nucleation and growth must take place in approximately 2 ms, before the whole bubble cloud is transported downstream by the mean flow field. As indicated by figure 7, these frequencies are independent of the flow velocity.

4.1. Bubble size distributions

PDA measurements were made between 5 and 200 mm downstream of the constriction. Since the constriction itself was manufactured in steel, locations less than 5 mm downstream were not accessible for the phase-Doppler anemometer. The measurements were restricted to the one half of channel where flashing occurs first. Measurements were taken at 20–25 locations per profile, with 3000 single events at each location. To recognize long-term fluctuations in the channel, each profile was repeatedly measured. Complete profiles were rejected if the results showed a systematic error, for example caused by temperature drifts of the test loop. Figures 8 and 9 show the number weighted size distribution and the size–velocity correlation obtained 20 mm downstream of the constriction 0.5 mm from the wall. Static pressure was 6.2 bar at a Re number of 128,000. A characteristic bubble size distribution can be seen with the peak point around 35 μm and a right-hand side tail of larger bubbles up to 200 μm. The arithmetic mean diameter D_{10} was 46.3 μm, while the Sauter mean diameter was 125 μm. As indicated by the solid line in the graph, no size–velocity correlation can be recognized.

Approximately 1600 different locations were measured, each giving the amount of information as indicated before. Therefore, it is sensible to reduce the data to characteristic parameters. For the size distribution, the following discussion will be based on the arithmetic mean diameter D_{10}, and the volume weighted mean diameter D_{30}. Nevertheless, the complete bubble size distribution was also stored in terms of distribution parameters. Here, it was found that the log–normal and, especially, the log–hyperbolic distribution (Xu *et al.* 1991) produce an excellent representation of all measured size distributions. Therefore, any change in the shape of the bubble size distribution may also be discussed in terms of changes of the parameters of the log–hyperbolic function.

In figures 10 and 11 the axial development of the radial profiles of D_{10} and D_{30} are shown between 15.0 and 100.0 mm downstream of the constriction at a pressure of 6.1 bar, corresponding to a saturation temperature of 20°C. Mass flux and Re number were 4720 kg/m^2/s and 104,000, respectively. Values of D_{10} between 50 and 80 μm and D_{30} between 75 and 120 μm were obtained, with a slight tendency to increase in the flow direction. In the radial direction, D_{10} increases almost monotonically from the centerline ($2y/h = 0$) to the wall ($2y/h = 1$), while D_{30} remains constant. This means that the size distributions become narrower near the wall.

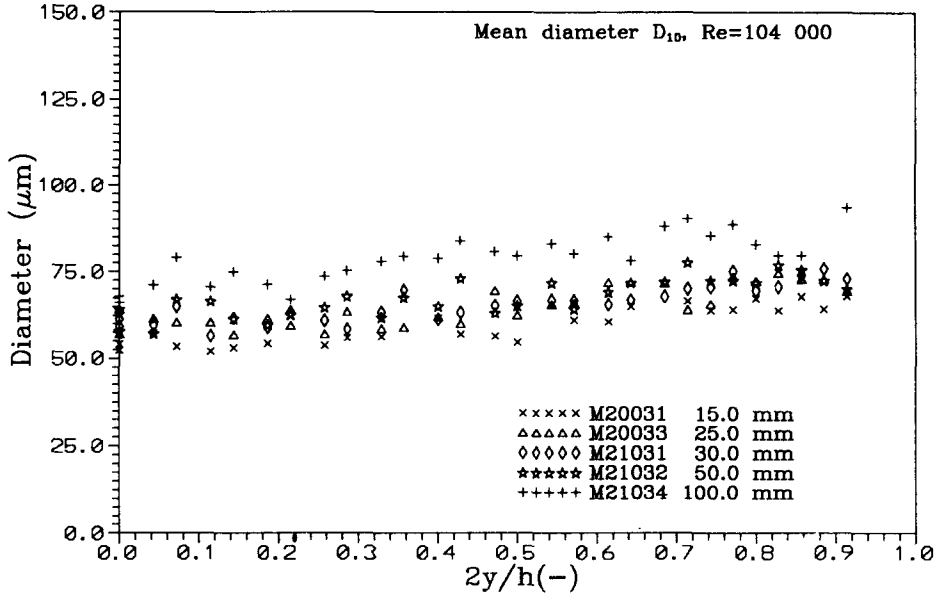

Figure 10. Axial development of number mean diameter D_{10}.

Since only a small increase of the mean bubble diameters in the axial direction was measured, it can be concluded that the major bubble growth took place inside the small recirculation zone. According to the present results, the complete process of bubble nucleation and growth must be finished within approximately 2 ms. Kocamustafaogullari (1983) formulated an equation for the size of steam bubbles detaching from a heated wall. Using the parameters of Freon 12 an initial bubble size of 29 μm can be estimated with this equation. According to Jones (1978), a further bubble growth rate of more than 50 μm/ms is possible, indicating that some agreement between measurements and theory exists. However, it must be kept in mind that these theoretical models were developed specifically for water–steam flows.

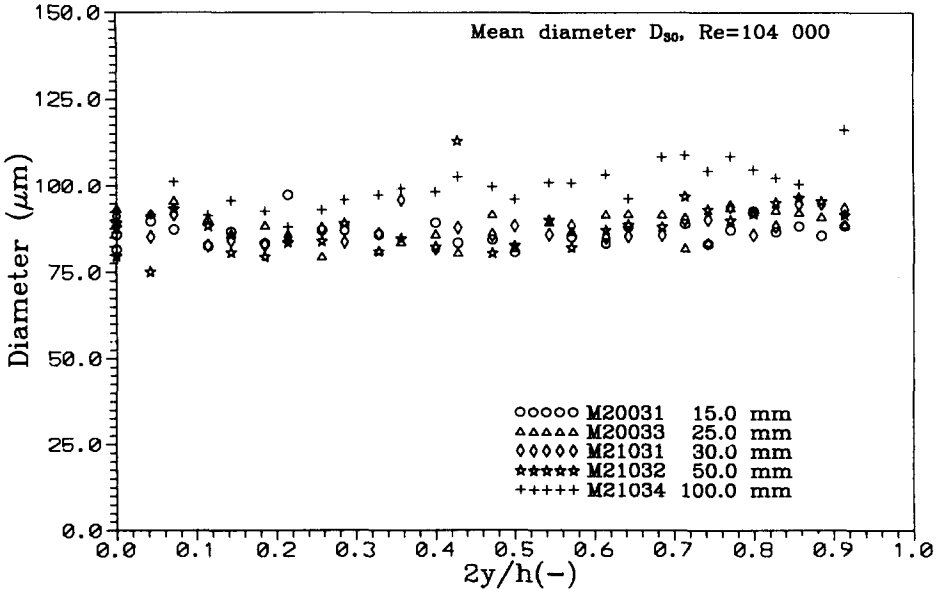

Figure 11. Axial development of volume mean diameter D_{30}.

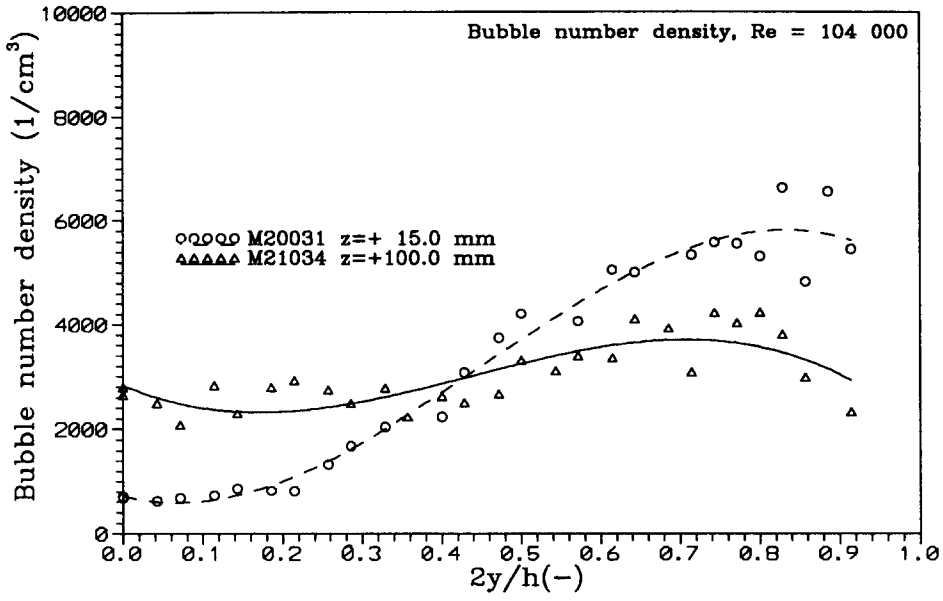

Figure 12. Profiles of bubble number density 15 and 100 mm downstream of the constriction.

4.2. Bubble number density and void fraction

Domnick *et al.* (1994) have shown recently, that particle number density and concentration can be measured by phase-Doppler anemometry, but the absolute accuracy of the results is typically not better than $\pm 30\%$. On the other hand, these experiments have demonstrated that relative changes of the concentration may be obtained very accurately. Moreover, a maximum particle number density exists, depending on the actual geometry of the phase-Doppler anemometer. For the system used in the present investigations this limit was found to be approx. 20,000 l/cm^3, which corresponds to a void fraction of 0.8% at mean bubble sizes of 60 μm. The measured number densities and void fractions shown below are representative values for a PDA measuring volume size of approximately 0.005 mm^3.

In figures 12 and 13 the radial profiles of the local bubble number density and the void fraction for distances of 15 and 100 mm downstream of the constriction are shown. As expected from the flow visualization results, the bubble number density 15 mm from the constriction is small near the channel centerline, but increases significantly towards the wall. Here, values of 6000 l/cm^3 were obtained at a Re number of 104,000. At 100 mm distance, the number density has already reached a certain equilibrium and is almost constant across the channel at a level of 3000 l/cm^3. The mean number density decreases by about 12% from 15 mm to 100 mm downstream of the constriction.

Again, the profiles of the void fraction confirm the results of the flow visualization studies. The measured void fraction increases from the channel centerline to the wall region, reaching maximum values of 0.3%. However, in contrast to the profiles of the number density, the void fraction does not decrease near the wall, but increases in the whole channel. This can be discussed also in terms of the mean void fraction, which rises by 33% from 0.12% at 15 mm to 0.16% at 100 mm. This difference in the behaviour of bubble number density and void fraction is due to the increase in the volume mean diameter of the bubbles. Most likely, small bubbles disappear again, while larger bubbles still increase in size. This is further supported by figure 14, in which the development of mean bubble number concentration and mean void fraction from 15 to 100 mm downstream of the constriction is shown.

Three different regions can be distinguished. Between 15 and 25 mm, both number density and void fraction increase, between 25 and 75 mm the void fraction is almost constant at decreasing values of the number density and from 75 to 100 mm the void fraction increases again, still accompanied by a decreasing bubble number density. It can be concluded that two different processes are responsible for this behaviour. Immediately behind the vena contracta, small bubbles

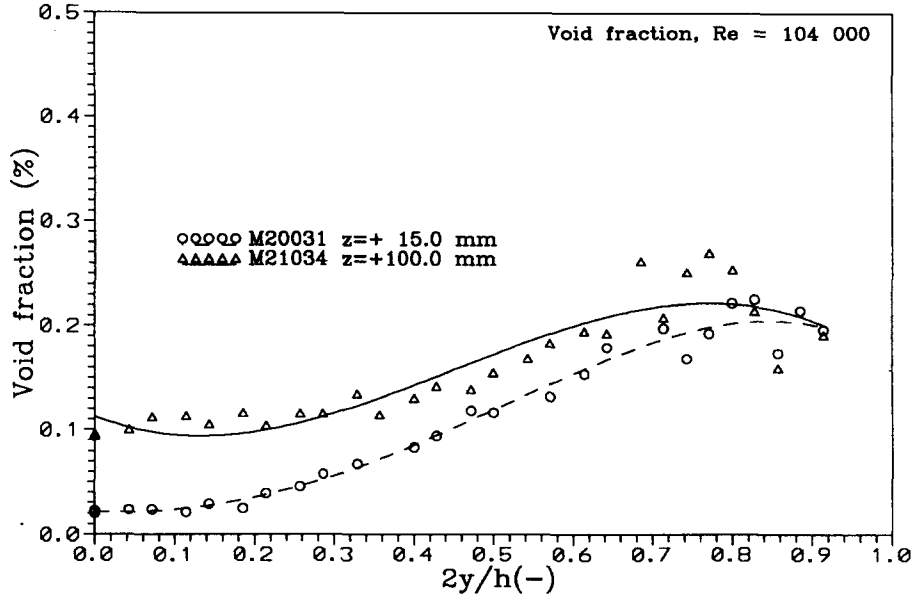

Figure 13. Profiles of void fraction 15 and 100 mm downstream of the constriction.

seem to condense when experiencing the slight increase in static pressure, further downstream, bubbles larger than a certain threshold diameter increase further in size due to the reduction of static pressure in vertical upflow.

4.3. Influence on the turbulent flow field

The influence of the nucleation and growth process of the bubbles behind the constriction on the flow field will be discussed by means of a comparison between single-phase and two-phase flow results. Since it was not possible to add seeding particles to Freon due to the influence on the nucleation process, the velocity measurements shown for flashing flow are overall mean values for the complete bubble size ensemble. The obtained results indicated only a very weak correlation

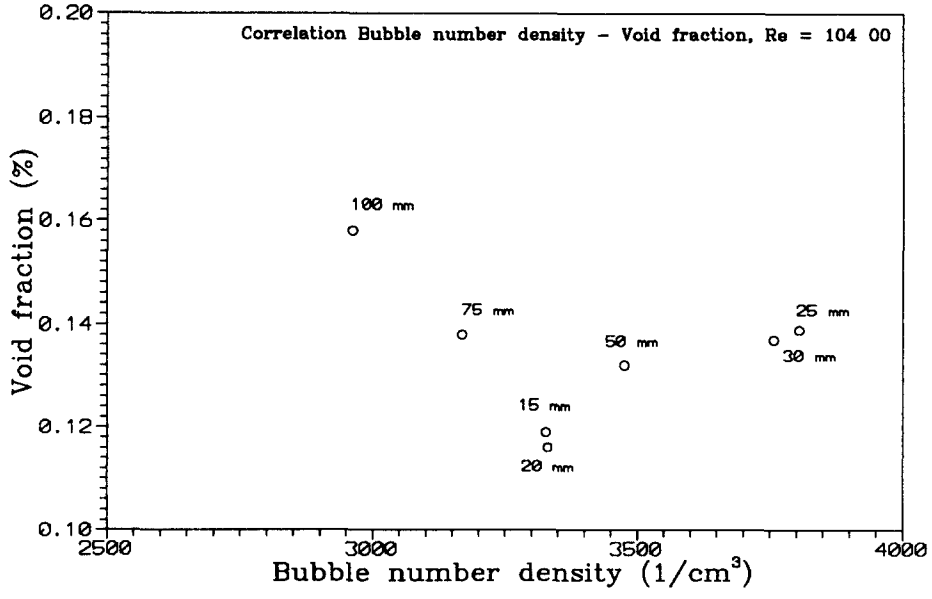

Figure 14. Correlation between number concentration and void fraction.

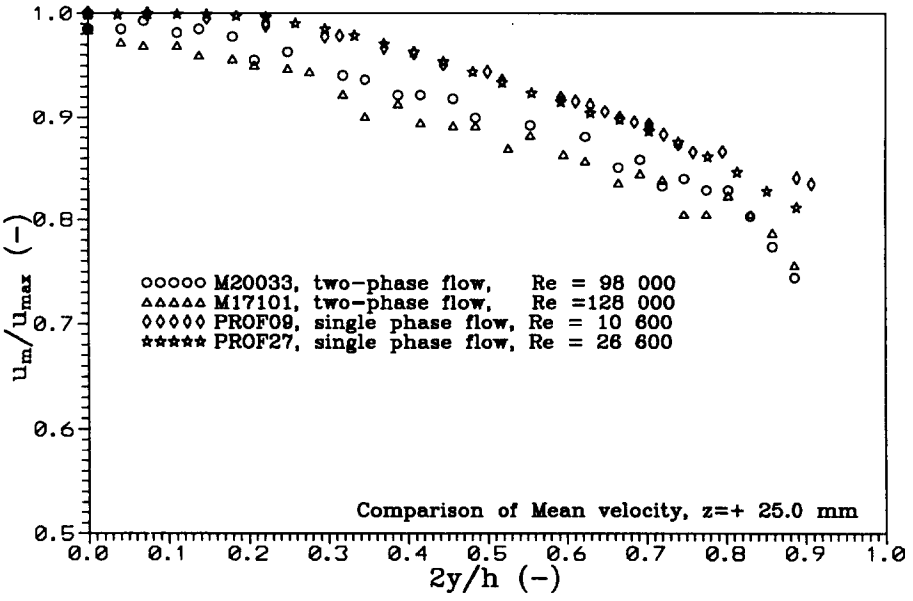

Figure 15. Mean velocity profile in single- and two-phase flow at $z = 25$ mm.

between bubble size and mean and rms velocity of the bubbles. The single-phase measurements were performed with water at Re numbers between 10,000 and 25,000. This should be high enough to establish a fully developed turbulent flow field in the channel. In figures 15–18 profiles of mean velocity and turbulence intensity 25 and 100 mm downstream of the constriction are shown. For single-phase flow, already 25 mm behind the constriction an almost fully developed turbulent profile is obtained with turbulence intensities varying between 5% on the centerline and 8% towards the wall. No significant differences between 25 and 100 mm can be seen, except a slight decrease of the turbulence intensity near the wall. Furthermore, the profiles for Re = 10,600 and 26,600 are almost identical.

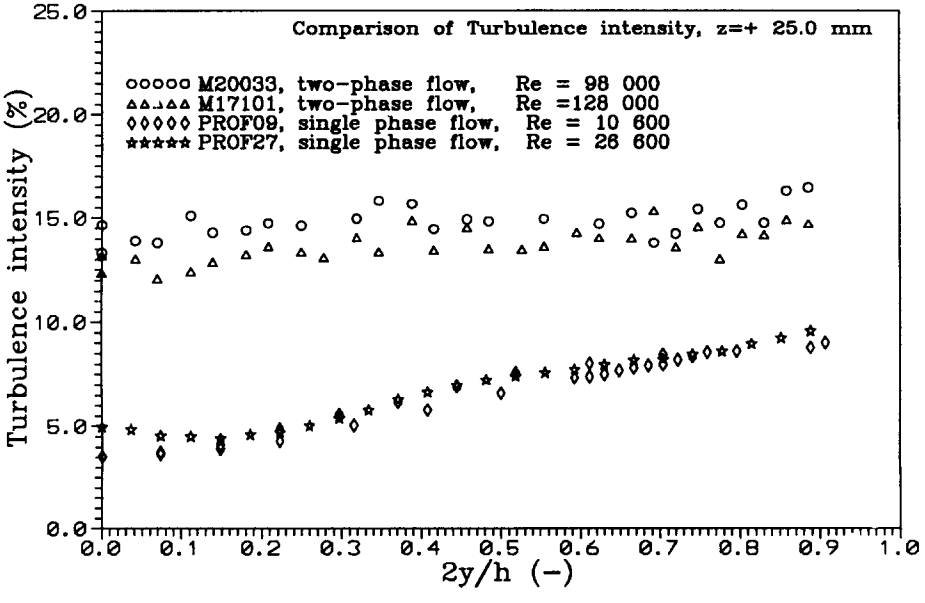

Figure 16. Profiles of turbulence intensity at $z = 25$ mm.

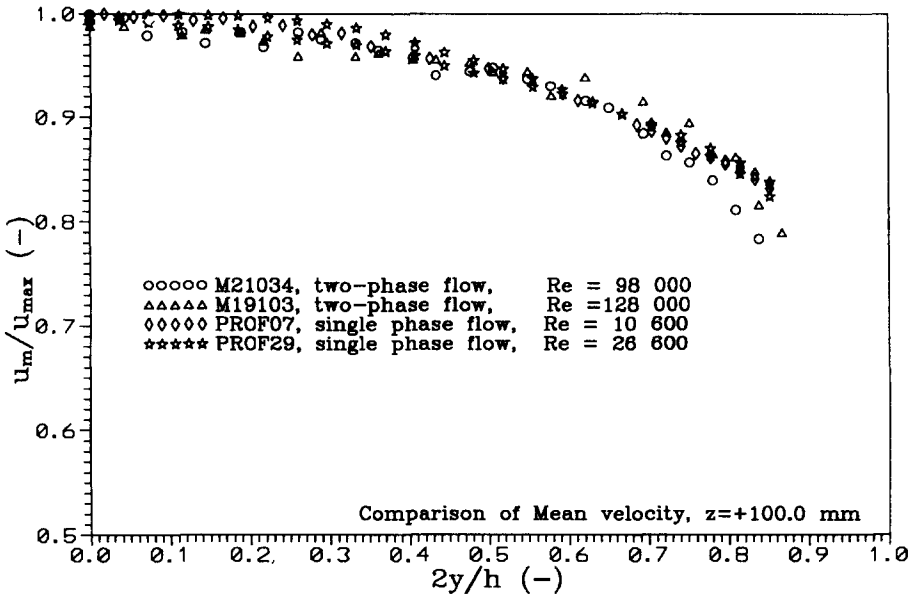

Figure 17. Mean velocity profile in single- and two-phase flow.

A completely different flow field is obtained when flashing of the flow occurs. At $z = 25$ mm, the mean velocity gradient is almost constant, leading to a sawtooth-like profile of the mean velocity. The turbulence intensities are 2 to 3 times higher than in single-phase flow with a much smaller gradient. At $z = 100$ mm (40 step heights downstream of the constriction) the mean flow fields are very similar, except that the gradient near the wall is somewhat higher in two-phase flow. However, the turbulence intensities in two-phase flow are approximately 50% higher, and it becomes evident that an influence of the Re number still exists, since the turbulence intensities at Re = 98,000 are considerably larger than at 128,000. It can be concluded, that the disturbances introduced by the flashing process immediately behind the constriction have a strong influence on the development of the turbulent flow field downstream. Here, a distinction must be drawn between

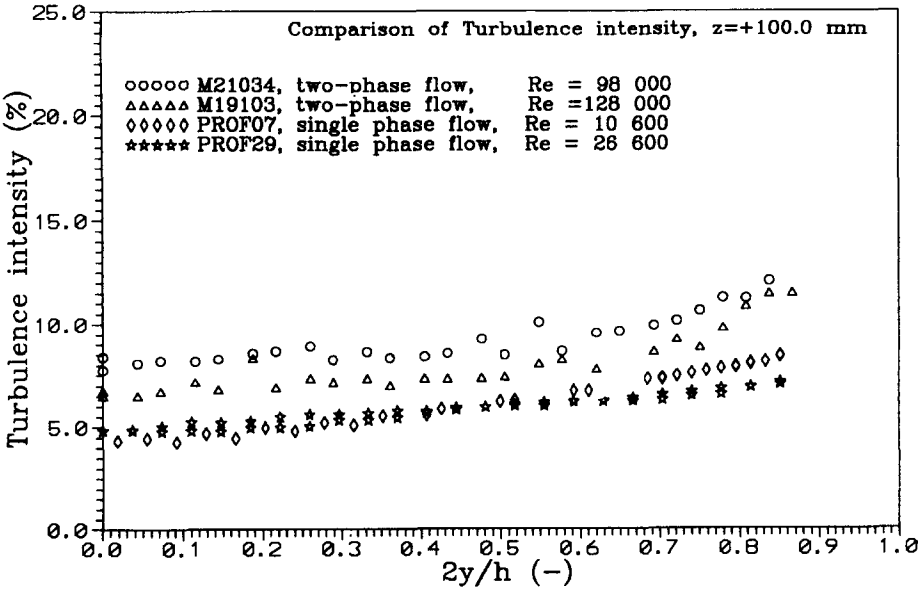

Figure 18. Profiles of turbulence intensity at $z = 100$ mm.

real turbulence and a periodic excitation of the mean flow field. The periodic growth and collapse of the recirculation zone with changes in the pressure distribution at the constriction will, most likely, tend to modulate the mean flow also. In future measurements, these effects will be further investigated by means of the frequency power spectra, in which low frequency components due to the fluctuating mean flow can be easily distinguished from real turbulence contributions. Unfortunately, the PDA system used herein was not able to store the necessary arrival times of the bubble events.

5. SUMMARY

The presented results have shown the possibility to use the laser light sheet technique and phase-Doppler anemometry to investigate the initial phase of flashing flow. Bubble sizes, number densities and void fractions behind a sudden constriction were measured and the influence of the bubble growth process on the flow field could been obtained. The results can be summarized as follows:

- Bubble nucleation and initial growth take place in the recirculation zone immediately after the constriction. Further downstream, small bubbles collapse again, while larger bubbles increase in diameter.
- The arithmetic mean bubble diameters 15 mm downstream of the constriction are in the range of 50 μm with a tendency to increase in the downstream direction. The size distributions can be successfully represented by the log–hyperbolic distribution.
- The mean bubble number density decreases again behind the vena contracta, while the void fraction increases due to an increase in the mean bubble size.
- The periodic growth and collapse of the recirculation zone influences the whole flow field behind the constriction and creates a fluctuating velocity component.

The obtained results may serve as initial conditions for the simulation of flashing flows. However, more detailed investigations are necessary to obtain a deeper insight into the processes. Future work will focus on two major topics:

- Measurements inside the recirculation zone to obtain the bubble detachment size and the nucleation site density. These will be made by phase-Doppler anemometry as well as flow visualization techniques.
- Measurements of frequency spectra in the flow field downstream of the constriction. This is necessary to be able to distinguish between turbulence and fluctuating mean velocities. However, these measurements will always suffer from the lack of seeding particles in the liquid phase.

Acknowledgements—The authors gratefully acknowledge the financial support of the present investigations by the Deutsche Forschungsgemeinschaft (DFG) through the Sonderforschungsbereich 222 "Heterogene Systeme unter hohen Drücken".

REFERENCES

Abuaf, N., Wu, B. J. C., Zimmer, G. A. & Saha, P. 1981 A study of non-equilibrium flashing of water in a converging-diverging nozzle. Report NUREG/CR 1864.

Bachalo, W. D. & Houser, M. J. 1984 Phase/Doppler spray analyzer for simultaneous measurements of drop size and velocity distributions. *Opt. Engng* **23,** 583–590.

Bauckhage, K. & Flögel, H.-H. 1984 Simultaneous measurement of droplet size and velocity in nozzle sprays. *2nd Int. Symp. on Appl. of Laser Anemometry to Fluid Mechanics*, Lisbon, Portugal.

Bilicki, Z., Kestin, J. & Pratt, M. N. 1990 A reinterpretation of the result of the Moby Dick experiments in terms of the non-equilibrium model. *Trans. ASME, J. Fluids Engng* **112,** 212–217.

Domnick, J., Ertel, H. & Tropea, C. 1988 Processing of phase/Doppler signals using the cross spectral density method. *4th Int. Symp. on Appl. of Laser Anemometry to Fluid Mechanics*, Lisbon, Portugal.

Domnick, J., Dorfner, V., Durst, F. & Hohmann, S. 1994 Spray propagation in pressure swirl atomization. *7th Workshop on Two-phase Flow Prediction*, Erlangen, Germany, 11–14 April.

Durst, F. & Zaré, M. 1975 Laser-Doppler measurements in two-phase flows. *Proc. LDA-Symp.*, Copenhagen, Denmark.

Jones, O. C. Jr 1978 Bubble growth in variable pressure fields. *Trans. ASME, J. Heat Transfer*, Vol. 100, No. 8, pp. 453–459.

Kocamustafaogullari, G. 1983 Pressure dependency of bubble departure diameter for water. *Int. Commun. Heat Mass Transfer* **10,** 501–509.

Naqwi, A. & Durst, F. 1989 Computation of light scattering from a dual-beam system. Internal Report LSTM/259/T/89, Lehrstuhl für Strömungsmechanik, Universität Erlangen-Nürnberg, Germany.

Pfeiffenberger, U. & Patil, M. 1978 Thermophysikalische Eigenschaften von Kältemitteln, Fortschrittsbnerichte der VDI-Zeitschriften, Reihe 6, No. 82.

Reocreux, M. 1974 Contribution à l'Etude des Débits critiques en Ecoulement diphasique. Thèse, l'Université de Grenoble.

Riznic, J., Ishii, M. & Afgan, N. 1988 Mechanistic model for void distribution in flashing flow. In *Transient Phenomena in Multiphase Flow* (Edited by Afgan, N. H.). Hemisphere, New York.

Sadatomi, M., Sato, Y. & Saruwatari, S. 1982 Two-phase flow in vertical noncircular channels. *Int. J. Multiphase Flow* **6,** 641–655.

Saffman, M., Buchhave, P. & Tanger, H. 1984 Simultaneous measurement of size, concentration and velocity of spherical particles by a laser-Doppler method. *2nd Int. Symp. on Appl. of Laser Anemometry to Fluid Mechanics*, Lisbon, Portugal.

Tanger, H. & Weitendorf, E.-A. 1989 Applicability test for the phase-Doppler anemometer for cavitation nuclei measurements. *ASME Int. Symposium on Cavitation Inception*, San Francisco, CA.

Xu, T.-H., Durst, F. & Tropea, C. 1991 The three parameter log-hyperbolic distribution and its application to particle sizing. *5th Int. Conf. on Liquid Atomization and Spray Systems*, ICLASS 91, Gaithersburg, U.S.A.